A&A 461, 81–93 (2007)
DOI: 10.1051/0004-6361:20066088

Astronomy & Astrophysics

Galaxy clusters in the CFHTLS

First matched filter candidate catalogue of the Deep fields⋆

L. F. Olsen[1,2], C. Benoist[2], A. Cappi[2,3], S. Maurogordato[2], A. Mazure[4], E. Slezak[2], C. Adami[4], C. Ferrari[5], and F. Martel[2]

[1] Dark Cosmology Centre, Niels Bohr Institute, University of Copenhagen, Juliane Maries Vej 30, 2100 Copenhagen, Denmark
e-mail: lisbeth@dark-cosmology.dk
[2] Observatoire de la Côte d'Azur, Laboratoire Cassiopée, BP 4229, 06304 Nice Cedex 4, France
[3] INAF - Osservatorio Astronomico di Bologna, Via Ranzani 1, 40127 Bologna, Italy
[4] Laboratoire d'Astrophysique de Marseille, UMR 6110 CNRS-Université de Provence, BP 8, 13376 Marseille Cedex 12, France
[5] Institut für Astro- und Teilchen Physik, Universität Innsbruck, Technikerstraße 25, 6020 Innsbruck, Austria

Received 21 July 2006 / Accepted 19 September 2006

ABSTRACT

We apply a matched-filter cluster detection algorithm to the Canada-France-Hawaii Telescope Legacy Survey (CFHTLS) *i*-band data for the Deep-1, Deep-2, Deep-3 and Deep-4 fields covering a total of 4 square degrees. To test the implemented procedure we carry out simulations for assessing the frequency of noise peaks as well as estimate the recovery efficiency. We estimate that up to $z \sim 0.7$ the catalogue is essentially complete for clusters of richness class $R \gtrsim 1$. The recovered redshifts are in general overestimated by $\Delta z = 0.1$ with a scatter of $\sigma_{\Delta z} \sim 0.1$, except at redshifts $z \gtrsim 1$ where the estimated redshifts are systematically underestimated. The constructed cluster candidate catalogue contains 162 detections over an effective area of 3.112 square degrees corresponding to a density of ∼52.1 per square degree. The median estimated redshift of the candidates is $z = 0.6$. The estimated noise frequency is 16.9 ± 5.4 detections per square degree. From visual inspection we identify systems that show a clear concentration of galaxies with similar colour. These systems have a density of ∼20 per square degree.

Key words. methods: data analysis – surveys – galaxies: clusters: general – cosmology: large-scale structure of Universe

1. Introduction

Clusters of galaxies, the most massive gravitationally bound systems in the Universe are located at the nodes of the cosmic web and are thus good tracers of the large-scale structures (e.g., Bahcall 1988; Huchra et al. 1990; Collins et al. 2000). Their intimate connection with the power spectrum of the initial density fluctuations as well as to the cosmological parameters make them important targets in observational cosmology (e.g. Bahcall et al. 1997; Oukbir & Blanchard 1997; Holder et al. 2001; Schuecker et al. 2003). Additionally, they are still accreting matter along filaments and even at $z = 0$ a large fraction of them do present signs of substructures in their morphology and in the galaxy velocity distribution. Therefore, a prerequisite for addressing any cosmological issue from a cluster sample is not only to have a large homogeneous sample with a well-understood selection function, but also a good understanding of cluster evolution including constraints on their dynamical state.

The evolution of galaxy clusters has in recent years obtained a lot of attention. This is partly due to the advent of large telescopes and sensitive instruments which allow to carry out detailed studies of high redshift systems. Many studies have concentrated on the colour of the red sequence galaxies. These have shown that most of the known systems exhibit properties similar to those of present day clusters (e.g., Stanford et al. 1997, 1998; van Dokkum et al. 2000; Lidman et al. 2004), when taking into account the passive evolution of the stellar populations. Most of the studied systems have been X-ray selected, which is likely to trace the most massive systems at any redshift. Therefore, the current studies may be biased towards old, well-evolved systems missing the true progenitors of present day clusters and galaxies (van Dokkum & Franx 2001). In order to better understand such biases and selection effects it is important to use different detection methods and wavelength regimes.

A number of different detection algorithms and wavelengths have been used for identifying systems at increasingly higher redshifts. The largest cluster samples have been constructed using either optical (e.g., Postman et al. 1996; Olsen et al. 1999b; Gladders & Yee 2001; De Propris et al. 2002; Postman et al. 2002; Goto et al. 2002; Kim et al. 2002; Gal et al. 2003; Bahcall et al. 2003; Miller et al. 2005; Tago et al. 2006) or X-ray (e.g., Böhringer et al. 2000, 2004, and references therein) data. More recently, the Sunyaev-Zeldovich effect has also been used for detecting clusters of galaxies (Carlstrom et al. 2002). Each method is based on one or at most a few characteristics derived from known clusters and may thus introduce biases against certain types of systems. Therefore, it is of utmost importance for each method to have a well-defined selection function including a clear understanding of the built-in biases. Furthermore, directly comparing catalogues covering the same area extracted by

⋆ Full Table 3 is only available in electronic form at the CDS via anonymous ftp to cdsarc.u-strasbg.fr (130.79.128.5) or via http://cdsweb.u-strasbg.fr/cgi-bin/qcat?J/A+A/461/81

different methods will yield important insight into the different biases introduced by the different methods.

The Sloan Digital Sky Survey (SDSS) data with its large area and multi-colour coverage, as well as complementing spectroscopic information, has recently provided an important test-bed for a number of optical cluster detection methods at low redshifts (e.g., Kepner et al. 1999; Kim et al. 2002; Goto et al. 2002). Thorough comparisons between the different methods have been carried out by Kim et al. (2002); Goto et al. (2002); Bahcall et al. (2003). These comparisons show that, not surprisingly, there are always differences between the various catalogues, part of which are caused by the different ways the parameters such as for example richness are estimated. The SDSS data are sufficient for detecting clusters to at most intermediate redshifts ($z \sim 0.5$). At higher redshifts only smaller data samples have been available, such as the KPNO/Deeprange survey by Postman et al. (2002) and the ESO Imaging Survey (Olsen et al. 1999a,b; Scodeggio et al. 1999). Recently, the Red sequence Cluster Survey by Gladders & Yee (RCS, 2005) covering 100 square degrees has been achieved thus starting to probe large volumes to high redshift. However, a detailed comparison of the efficiency of different methods at high-z has yet to be carried out.

For detailed comparison between different methods, wide, deep and preferentially multi-passband homogeneous surveys are required in order to provide the necessary data for a number of different detection methods. The design of the Wide survey of the Canada-France-Hawaii Telescope Legacy Survey (CFHTLS) provides a data set that is particularly well-suited for carrying out such studies. This survey is currently underway and is planned to cover ∼170 square degrees in 5 passbands spread in 4 patches with limiting magnitudes up to $25^{\rm m}$. It will provide the necessary ground for building a large, well-controlled cluster candidate sample at redshifts $z \lesssim 1.3$, derived from a set of different search techniques using the spatial as well as photometric properties in one or more passbands. Such catalogues will allow us to test accurately the $z > 0.5$ component of the cluster distribution. Using automatic search techniques will allow us to build selection functions for each of our independently extracted catalogues. A careful comparison between the various independently extracted cluster samples will allow us to understand the additional difficulties in detecting clusters at successively higher redshifts as well as improve our knowledge about clusters at these redshifts. Combining the catalogues from several searches we will create a robust cluster sample well suited for both cosmological and galaxy evolution studies.

This paper is the first in a series describing detection and investigations of primarily the photometric properties of the identified systems. In this first paper we describe our implementation of the matched filter detection method which we apply to the $i-$band data of the Deep Survey of the CFHTLS. The depth presently reached by the Deep CFHTLS corresponds roughly to the final depth of the Wide part of the survey. Furthermore, the small size of the Deep provides a good test-bed for various detection algorithms for investigating the potential of the Wide survey. The motivation for exploring the $i-$band in this first paper is two-folded: first, the survey area is planned to be covered by $i-$band as high priority, later followed by the other passbands; second, most previous optical cluster searches have been carried out in $i-$band, thus focusing on this filter facilitates comparisons with previous surveys minimising the effect of the variation in wavelength. In future papers we will apply the same algorithm to data in other passbands in order to investigate how sensitive this technique is to the choice of passband at different redshifts.

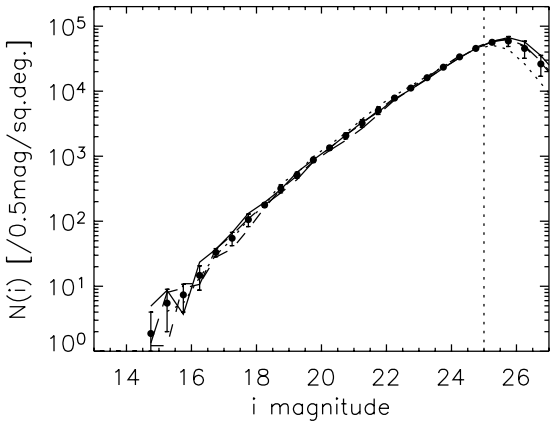

Fig. 1. Average galaxy number counts (filled dots with error bars) for the four Deep fields in the $i-$band. The number counts for the individual fields are shown as follows: D1 – solid line; D2 – dotted line; D3 – short-dashed line; and D4 – long-dashed line. The vertical dotted lines denote our adopted magnitude limit for the present analysis.

To investigate the advantages of using additional colour information we will apply a colour search technique to the same data and cross-compare the detections between the different methods. In parallel we are working on detection methods based on photometric redshift slicing to fully exploit the multi-passband data for identifying structures, as well as on searches based on weak lensing studies (see Gavazzi & Soucail 2006). In future papers we will also characterize the detected systems in terms of total luminosity, concentration, shape parameters and colour properties such as the existence and significance of the red sequence.

The present paper is structured as follows: in Sect. 2 we describe the galaxy catalogues used in the present work. These catalogues are a modified version of the Terapix CFHTLS galaxy catalogues. Section 3 describes the matched-filter cluster identification method which is an improved version of that implemented for the ESO Imaging Survey (Olsen et al. 1999a). This section also describes a series of simple simulations to account for the rate of false-positives as well as the selection function. In Sect. 4 we apply the detection to the $i-$band galaxy catalogue of the four Deep fields of the survey covering a total of ∼4 square degrees and compare the constructed cluster catalogue to those of previous works. In Sect. 5 we summarize our findings.

Throughout the paper we use a cosmological model with $\Omega_{\rm m} = 0.3$, $\Omega_\Lambda = 0.7$ and $H_0 = 75\,{\rm km\,s^{-1}Mpc^{-1}}$.[1]

2. Galaxy catalogues

The galaxy samples used in this work are obtained from the catalogues released by the Terapix team as part of the CFHTLS release T0002 in August 2005[2]. The released catalogues are extracted with SExtractor using a *gri*-chi-squared image (Szalay et al. 1999) as reference and measuring magnitudes in each individual band. Here we concentrate on the $i-$band catalogues of the four Deep fields with a total sky coverage of 4 square degrees. The 80% completeness limits of the catalogues are reached at magnitudes of $i = 24.8$–25.4. Starting from the release catalogues we apply our own star-galaxy separation based on the locus of the objects in a half-light radius versus magnitude diagram, where the stars are clearly separated from the galaxies at magnitudes $i \lesssim 21$–22. Furthermore, we apply a correction for

[1] We use $h_{75} = \frac{H_0}{75{\rm km\,s^{-1}Mpc^{-1}}}$

[2] `http://terapix.iap.fr/rubrique.php?id_rubrique=198`

Galactic extinction based on the maps by Schlegel et al. (1998). As part of the release, the Terapix team provides mask files for filtering out false detections, usually caused by saturated stars or ghost images. Those masks are produced based on the *i*-band images. We have visually inspected the images together with the masks and, in areas where spurious detections caused by ghost images or spikes from bright objects were still present, defined a few additional masks.

In Fig. 1 we show the galaxy number counts obtained for these post-processed catalogues for the four Deep fields. The average counts are shown as points with error bars computed as the standard deviation between the fields. It can be seen that the D2 field is slightly shallower than the others as was also indicated by the 80% completeness limiting magnitudes as given by the Terapix team (24.8–25.4). It can be seen that the 80% completeness limits roughly corresponds to the peak of the counts. As a compromise we choose in all fields to use galaxies with $i \leq 25$. This limit is also indicated in the figure.

3. Cluster detection

The cluster detection algorithm used in the present paper is based on the matched-filter technique (e.g., Postman et al. 1996) as it was implemented for the ESO Imaging Survey (Olsen et al. 1999a). To this version a number of improvements have been added for the present work. Here, we summarize the main aspects of the implementation, in particular focusing on the new implementations done for this work.

3.1. Matched-filter cluster detection

The matched-filter detection procedure is based on a maximum likelihood analysis with the following steps:

1. creation of a filter based on an assumed cluster galaxy luminosity function and radial profile;
2. creation of likelihood maps for a series of redshifts;
3. detection of significant peaks;
4. cross-matching of peaks for different redshifts;
5. creation of likelihood curves and identification of the redshift of maximum likelihood used for defining the cluster properties such as redshift and richness.

The current implementation uses the Postman et al. (1996) matched-filter algorithm, which filters the galaxy catalogue based on positions and apparent magnitudes. The filter is constructed to enhance galaxy overdensities that resemble that of a cluster with the assumed radial profile and luminosity function (LF) embedded in a background of field galaxies. We have adopted the Hubble radial profile characterized by a core and a cut-off radius. The LF is a Schechter function (Schechter 1976) characterized by the faint-end slope and Schechter magnitude, M^*. The chosen values for these parameters are taken from Popesso et al. (2005) and listed in Table 1 after conversion to our cosmology. For details of the matched filter algorithm and its variants we refer the reader to Postman et al. (1996); Kepner et al. (1999); Olsen et al. (1999a) and Kim et al. (2002).

The matched filter is applied to observed quantities (thus angular distances and apparent magnitudes). The filter is computed in a grid covering the galaxy catalogue, where we have chosen the pixel scale to correspond to half the core radius. To construct the likelihood curves the filter is tuned to a series of redshifts from $z = 0.2$ to $z = 1.3$ in steps of $\Delta z = 0.1$ and applied to the galaxy catalogue for each of them. The useful redshift range depends on the passband and the depth of the data. To derive the apparent Schechter magnitudes we have used k-corrections derived from model spectra for an elliptical galaxy from the Coleman library (Coleman et al. 1980), thus ignoring luminosity evolution of the galaxies. The main impact of this is that redshifts of the clusters may be biased low for the high-z part of the sample.

Table 1. Detection and filtering parameters for building the cluster catalogues.

Parameter	Value
Filter	
Core radius, r_c	$0.133\,h_{75}^{-1}$ Mpc
Cut off radius, r_{co}	$1.33\,h_{75}^{-1}$ Mpc
Faint end slope of LF, α	–1.15
Schechter magnitude, M_i^*	–22.24
Likelihood maps	
Pixel scale	$0.5r_c$ = 21.6–8.5 arcsec
z-interval	0.2–1.3, $\Delta z = 0.1$
Peak detection	
Threshold	3.5σ
Minimum area	$\sim\pi\,(r_c(z)/2)^2 \sim 4$pixels
A posteriori filtering	
Minimum number of shells	2

As discussed in Sect. 2, each galaxy catalogue has an associated mask file usually masking false detections around saturated stars or ghost images. Since such false detections often come in fairly dense groups, they are very efficiently detected by the cluster finding algorithm. To avoid such false cluster detections, objects within masked regions are discarded in the analysis. While it is of course important to avoid spurious cluster detections caused by false objects within these masks, the masking of regions creates holes in the galaxy distribution, which in turn hampers the assumption for the matched filter algorithm of a homogeneous background. This has to be taken into account both when estimating the background as function of magnitude (in this case in particular the density of background objects) and when evaluating the filter in the vicinity of the masked areas. The lack of objects will decrease the signal compared to the ideal case of complete coverage, thus the clusters situated in the affected regions will have a lower probability of being detected. As a result of the spatial extent of the applied filter, the regions affected by the holes are not only the masked regions but also their immediate vicinity. Due to the larger angular extent of the filter at low-z, the holes affect larger regions in the low-redshift shells than in the higher redshift domain. This may in the end cause large regions of the catalogue to be significantly incomplete. To diminish the effect of the holes in their vicinity we add randomly distributed galaxies to fill the holes in the filtered galaxy catalogues before applying the matched-filter algorithm. The density of the added galaxies corresponds to the average density of the field.

Analogously, the signal at the edges will be decreased due to the lack of galaxies outside the observed regions. To counteract this effect we also add a border of randomly distributed galaxies again with a density corresponding to the average in the field. The width of the added frame corresponds to the extent of the largest filter radius corresponding to the one used for $z = 0.2$. The magnitude distribution of the added mock galaxies is the one of the catalogue itself. Of course, this approach can never fully recover the signal of a partially masked cluster or a cluster situated at the limit of the survey, but it assures that the background signal is kept constant across the field allowing a more homogeneous detection over the entire area.

For each redshift, a likelihood map with the pixel scale corresponding to half the core radius at this redshift is created. The maps are stored as FITS files to facilitate the use of standard image analysis tools (here we use SExtractor, Bertin & Arnouts 1996) for detection and characterization of the peaks. Even though the masked areas are filled, the signal in these regions is useless, and therefore we use weight maps to discard these regions in the peak detection. The weight maps are created with the same pixel grid as the likelihood maps starting from the updated mask files for each field. To avoid splitting clusters with substructures we do not use the deblending option of SExtractor, even though this probably reduces the sensitivity to clusters close to the same line of sight.

After peak detection, the significant peaks in the different maps, corresponding to different redshifts, are cross matched using the association program of the LDAC-tools[3]. This tool associates detections by their position, such that, if the detection areas in two shells overlap, the detections are associated to each other to create the raw likelihood functions.

Due to the slow variation of the appearance of clusters with redshift and the luminosity width of the filter, a cluster causes a significant peak in a number of consecutive shells. It is not likely that a cluster absent in one shell is recovered at a more distant redshift. Therefore, the raw likelihood functions are analysed and split in two if it occurs that for a given redshift no detection is found. In this way it is assured that all likelihood curves are contiguous as is expected for real clusters. Additionally, since the filter size is much larger at low redshifts than at higher redshifts it may happen that two detections are blended at low redshift but deblended at higher redshifts. The raw likelihood curves are therefore searched for shells where two detections are associated to the same cluster. In such cases only the detection closest to the foreground one is kept in the present detection and the other one used in a new series of detections. Both of these procedures are improving the sensitivity to clusters along the same line of sight.

The above process creates the final likelihood curve for each cluster candidate. Again due to the persistency of real clusters we require a detection to appear in at least two consecutive redshift bins in order to be considered further. The properties of the cluster candidate are determined from the redshift at which the likelihood signal is maximized. The cluster position is taken to be the position of the maximum signal.

Compared with the implementation for the EIS project, the main improvements are the handling of masked regions in the galaxy distribution as well as the diminishing of the edge effects using randomly distributed galaxies. Also, the analysis of the likelihood curves has been improved. The EIS implementation was using what we here call the raw likelihood curves.

3.2. Balancing real and false detections

When constructing a cluster candidate catalogue, the aim is to identify as many real systems as possible while discarding chance alignments. As it is clear from the above description there are a number of steps where parameters have to be selected by the user in order to optimize this balance. When the pixel scale has been chosen, among the remaining parameters are the detection threshold and minimum accepted area used by SExtractor. These parameters are related to the "raw" peak detection in the likelihood maps. After constructing the raw catalogues several parameters may also be useful to suppress the noise contribution.

[3] Leiden Data Analysis Center,
ftp://ftp.strw.leidenuniv.nl/pub/ldac/software

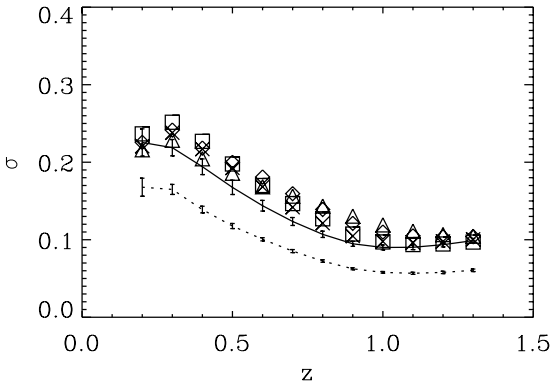

Fig. 2. Variation of standard deviation of the likelihood map pixel value distributions as function of redshift. Each of the Deep fields are represented by individual symbols (diamonds for D1, triangles for D2, squares for D3 and crosses for D4). The lines denote the average over 20 mock catalogs with the error bars giving the standard deviation. The solid line marks the relation for the "correlated" background catalogues and the dotted line that of the "uniform" background catalogues.

For instance, since clusters are expected to persist through more than one redshift shell we demand the candidates to show up in at least two consecutive shells. Even though we use the number of redshift bins contributing to the likelihood curve, other parameters such as signal-to-noise or richness could also be important discriminators.

In principle, the optimum way for addressing this point is by using mock galaxy catalogues like the ones produced in *N*-body simulations including the full hierarchy of structures. For such a catalogue one would know the precise location of clusters as well as their physical properties. Therefore, application of the cluster detection to such catalogues would allow at the same time to identify how many clusters were detected and how many additional detections, caused by superposition effects, were found. Hence one could immediately balance the false and real detections based on the same simulated catalogues. However, in reality the simulation of the galaxy distribution as well as identifying galaxy systems is a complex task, which will be investigated in a future paper.

Here, we adopt a simpler approach simulating separately the distribution of the background and cluster galaxies, whereby we have full control of the input parameters of the clusters and thus not only the recovery rate, but also the precision of the estimated parameters can be directly assessed.

To build backgrounds as realistic as possible means reproducing both the magnitude distribution of galaxies and their spatial distribution properties. In this process we encounter a coherence issue since a fair reproduction of the clustering of galaxies (in particular at small scales) would mean that clusters are naturally built in. However, densities and clustering amplitudes can be reproduced in spatially independent bins of 1 mag. Such a procedure allows then to limit the luminosity coherence of a possible clump to 1 mag, whereas a real cluster is expected to span over a much larger magnitude range. A set of correlated backgrounds have been constructed based on the algorithm by Soneira & Peebles (1978), allowing to reproduce fairly well the slope of the two-point correlation function as well as its amplitude as a function of magnitude. Our reference for the number counts and correlation functions are those measured directly from the D1 field. Besides the correlated backgrounds we also created for comparison spatially uniform backgrounds reproducing

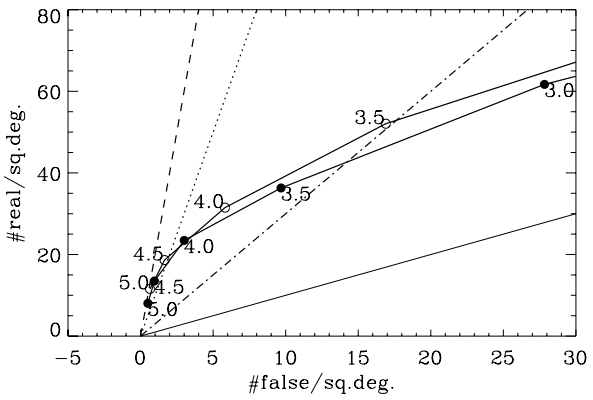

Fig. 3. The number of real and false detections per square degree for different detection thresholds and minimum area. The number of false detections is estimated from the correlated background catalogues. The upper curves with open symbols give the numbers for the minimum area corresponding to $\pi(0.5r_c)^2$ and the lower curves with filled symbols those for $\pi(1r_c)^2$. The numbers at each point mark the "n" in the "$n\sigma$" scaling of $\sigma_{\rm det}$. The thin solid line marks the locus of equal number of false and real detections. The dashed, dotted and dot-dashed lines mark a fraction of 5% , 10% and 33% false detections, respectively.

only the galaxy number counts. For each type of backgrounds 20 simulations were built.

For balancing the number of false and real detections, we applied the matched-filter algorithm to the four Deep fields as well as to each of the two sets of simulated catalogues. To investigate the impact of the clustering properties on the likelihood maps, and thus on the peak identification, we first compare the standard deviations of the pixel value distributions. In Fig. 2 we show this comparison for each redshift bin. For the simulated backgrounds we use the mean standard deviation in each bin while for the real data each catalogue is shown by an individual symbol. It can be seen that in general the standard deviations of the real data are larger than those of both of the two types of mock background catalogues. This is expected since in the real data the presence of clusters increases the density variations, and thus the variation in the pixel values. While the uniform backgrounds, as expected, show much smaller variations, the clustered background values represent well the lower limit of the standard deviation found in the real data.

When determining the detection threshold to be used for the peak identification one would like to use the standard deviation of the background pixel distribution of each likelihood map and set the threshold in a standard "$n\sigma$" fashion. However, due to the variations in clustering the background standard deviation varies as was seen above. In order to have a common reference for the background standard deviation, we used those derived from the average of the 20 correlated mock catalogues since these appear to represent a clustered background well. Hence, in the following the detection threshold scaling, $\sigma_{\rm det} = n\sigma$, will refer to the values of the average of the standard deviations, σ, of the 20 correlated background mock catalogues.

Having defined this reference it is now possible to compare the number of detections in different cases to define the optimum detection threshold and minimum area. The two key issues are to keep the fraction of false-positives low, while keeping a high detection efficiency. The first issue relates to the number of detections in the background only simulations and the second to the number of detections in the data catalogues. To have a fair representation of the number of false detections we use the correlated backgrounds for these estimates. The comparison of the number of detections in the real data and in the correlated backgrounds is shown in Fig. 3. It shows the number of detections in the real data versus the number of detections in the background catalogues for different settings of the detection threshold and minimum area. Even though the clustered background catalogues seem to represent the background well, it is possible that the noise fraction in this way is slightly overestimated. This (slight) overestimate is caused by the fact that the catalogue is built in slices of one magnitude and therefore concentrated clumps of galaxies with very similar magnitudes may be included despite the wrong luminosity function of the system. However, we expect this to be a minor effect, since the correlation of position and magnitude is limited to a relatively small magnitude range of one magnitude.

The most efficient suppression of the false detections is in the steepest part of the curves. When it turns flatter the detections in the catalogues become more noise contaminated. Therefore, the most efficient threshold judged from this relation alone is where the curves bend off. From the figure it can be seen that the choice of minimum area is not an efficient noise discriminator and thus to ensure the detection of the most concentrated systems (often being those at the highest redshifts) we choose to use the small minimum area corresponding to $\pi(0.5r_c)^2$. From the bending of the upper curve it can then be seen that a threshold of 4.0σ, corresponding to ∼20% false detections for a total of about ∼30 detections per square degree would be the most efficient in terms of rate of false-positives. However, other considerations such as completeness as function of redshift have to be taken into account as well. For investigating this we compare the resulting catalogues using both the 4.0σ and 3.5σ detection thresholds. In the latter case the total number of detections is ∼50 with ∼30% false detections.

We have carried out two comparisons: one internal between the two catalogues and one to an external cluster sample. First we visually inspected all the candidates in the 3.5σ (162 candidates) and 4.0σ (98 candidates) catalogues and found that 122 from the 3.5σ catalogue were graded A or B (see Sect. 4 for a definition) corresponding to the most reliable candidates. Of those candidates ∼43% are not included in the 4.0σ catalogue. A large fraction of these missing candidates were identified at high redshift, a main target of the present survey. Therefore, we consider the 3.5σ threshold a good compromise despite the increased frequency of false-positives. This choice is supported by the results of comparing to the XMM Large-Scale Structure Survey sample (XMM-LSS, Pierre et al. 2006) as discussed in Sect. 4.2. We find that all their $z \geq 0.5$ detections are missed if we use the 4.0σ detection threshold, but included using 3.5σ, which is our choice for the rest of this paper.

3.3. Towards a selection function

Having determined the optimum detection parameters it is important to investigate the recovery rate as function of redshift and richness (selection function). For building the selection function it is necessary to have control on the location of clusters as well as their basic properties. Therefore we have created simulated galaxy catalogues based on the background catalogues described above and clusters with the same characteristics (radial profile and LF) as the one used for the detection filter. A similar approach has been used by many authors for estimating recovery efficiency (e.g. , Kepner et al. 1999; Lobo et al. 2000; Goto et al. 2002; Kim et al. 2002; Postman et al. 2002).

Table 2. The relation between the input $\Lambda_{\rm cl}$-richness and the Abell richness classes. For the transformation between the counts and richness class we use the relation found by Postman et al. (1996).

$\Lambda_{\rm cl}$	$\langle N_R \rangle$	R
10	15	< 0
20	24	0
30	31	0
40	38	1
50	45	1
60	50	1
70	56	1
80	62	2
90	67	2
100	72	2
150	95	3
200	118	3
250	137	3
300	156	4

For each background setup we create 20 mock catalogues to which we add clusters with redshifts in the range 0.2–1.3 and $\Lambda_{\rm cl}$-richness from 10–300, as detailed in Table 2. The simulated clusters are built to resemble the model cluster used to construct the detection filter. In each field we add 12 clusters with different redshifts from $z = 0.2$ to $z = 1.3$, but constant richness. For each richness we construct 20 such catalogues. Altogether a set of 280 galaxy catalogues including clusters were produced, containing a total of 3360 galaxy clusters. Figure 4 shows one example of a set of 12 clusters with richness $\Lambda_{\rm cl} = 100$ ($R \sim 2$) embedded in a field background. From the figure it can be seen that at the highest redshifts the number of galaxies included in the catalogue is very small, therefore the contrast of the cluster against the background decreases significantly with redshift even for these fairly rich systems. It is also clear that it is more difficult to identify the clusters on the clustered background than on the uniform one, due to the larger number of background superpositions. The conversion between the input $\Lambda_{\rm cl}$-richness, the Abell richness counts, N_R (number of galaxies with magnitudes in an interval of size 2 mag limited at the bright end by the third brightest magnitude) and Abell richness class, R, is given in Table 2.

In order to determine the recovery rate, we apply the detection procedure to these mock galaxy catalogues and identify clusters around the nominal cluster positions. We use a search radius of 1.′5. We reject detections that have a matching detection (in terms of position and redshift) in the corresponding background galaxy population. In Fig. 5 we show the computed recovery efficiency as function of redshift and richness. From this figure and Table 2 it can be seen that, overall, these settings allow clusters with Abell richness class $R \gtrsim 1$ to be detected up to redshifts $z \sim 0.7$ with at least 80% efficiency, while at $z \gtrsim 1$, systems with $R \gtrsim 2$ are detected at 80% completeness.

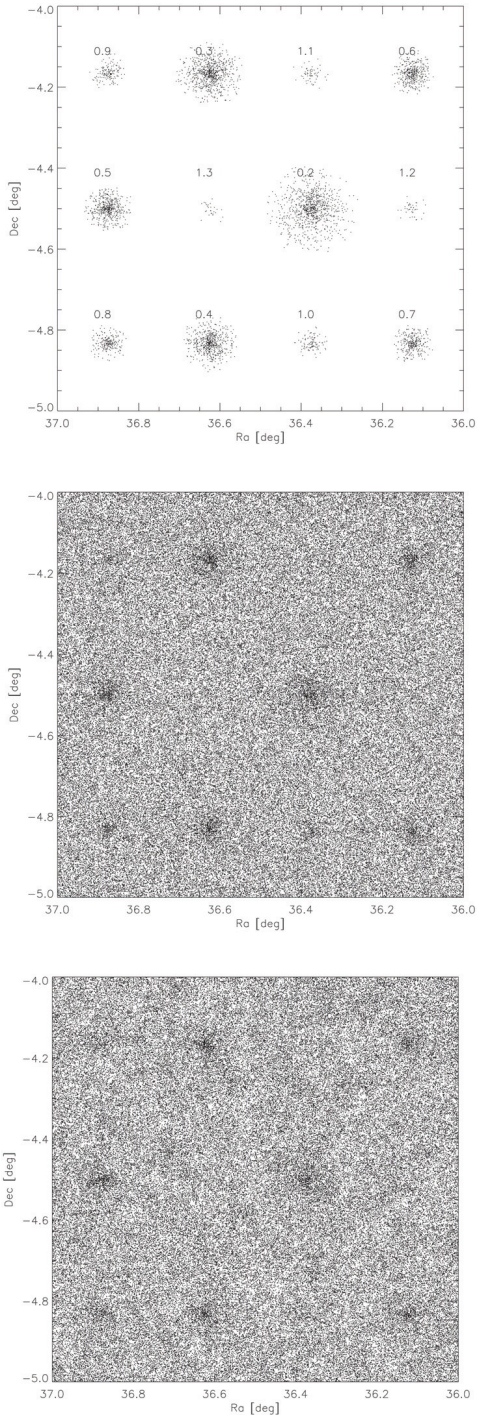

Fig. 4. An example of a simulated galaxy catalogue for the clusters only (*upper panel*), embedded in the uniform (*middle panel*) and correlated (*lower panel*) backgrounds. In all cases the catalogues are cut at the limiting magnitude of $i = 25$. The clusters all have a richness of $\Lambda_{\rm cl} = 100$ ($R \sim 2$) and the redshifts indicated in the upper panel.

3.4. Recovery of properties

In the previous section we discussed the efficiency of detecting a cluster at the position of the simulated clusters. Another important question for using the constructed cluster catalogue is the accuracy of the estimated cluster properties.

The first property we investigate is the accuracy of the recovered positions. In Fig. 6 we show the mean offsets as function of redshift and richness (upper to lower curve) and compare it with the core radius (smooth dotted line). We have chosen to limit ourselves in redshift and richness to cases where at least 50% (10 cases) of the 20 input clusters are recovered. This is done in order to make sure that we do not estimate the offsets on one special case but obtain a reasonable statistical significance. It can be seen that the average offsets from the nominal position is of the order or sligthly larger than the core radius for all richnesses. Here the detections are recovered within 1.′5 from the input center.

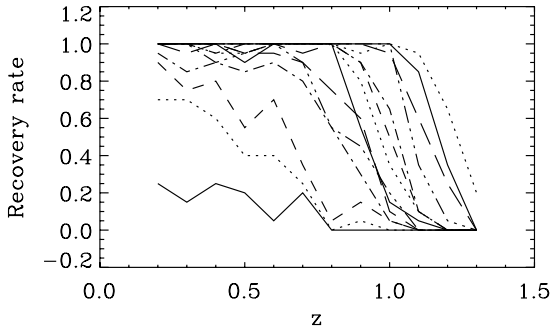

Fig. 5. The detection efficiency for the correlated background $\sigma_{\rm det}$ = 3.5σ, area $\sim \pi(0.5r_{\rm c})^2$. The lines correspond to $\Lambda_{\rm cl}$ = 10–300 from left to right.

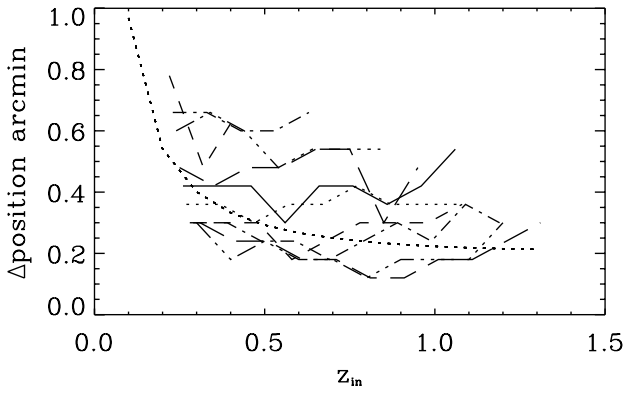

Fig. 6. The average matched-filter position offset as function of redshift and richness using a search radius of 1.5 arcmin. The different lines correspond to different richness as in Fig. 5. The smooth dotted line gives the corresponding angular extent of the core radius. We only include cases with at least 50% recovery.

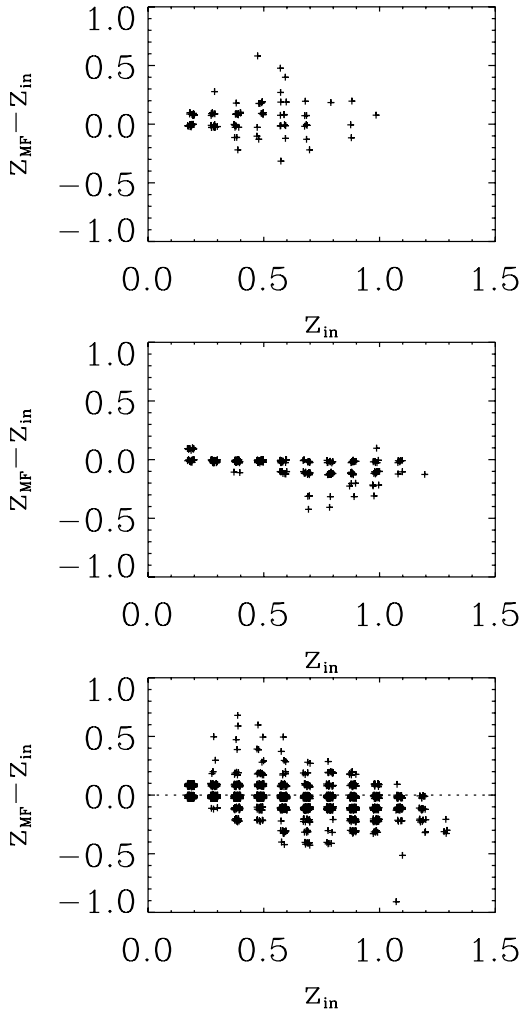

Fig. 7. Redshift offsets as function of input redshifts for richnesses of $\Lambda_{\rm cl}$ = 30 (*upper panel*), 150 (*middle panel*) and combined for all the investigated richnesses (*lower panel*). Each point is slightly offset by a random number to allow all points to be seen despite the discrete nature of the redshift measurements.

The main properties estimated by the matched filter algorithm are the redshift and richness. To investigate the accuracy of these estimates, we use the same matching as above adopting a search radius of 1.′5. In Fig. 7 we show the redshift offsets between the input and recovered redshifts for each of the recovered clusters mixing all richnesses in the lower panel. The two top panels give the offsets for richnesses of $\Lambda_{\rm cl}$ = 30 and 150. It can be seen that in general the recovered redshifts are in good agreement with the input ones, even though the scatter increases for the poorer systems. Furthermore, in the lowest redshift bins there is a tendency of overestimating the redshift while in the highest redshift end the opposite effect is seen. Since the mock clusters are constructed using no-evolution k-corrections, this effect is not the same as mentioned in Sect. 3.1, but is an additional offset introduced by the method. As discussed by Schuecker & Böhringer (1998) this may be an effect of the adopted algorithm and other choices could possibly perform better in this respect. However, it is worth noting that spectroscopic confirmations of clusters at low redshift detected in the EIS program confirm the consistency between real and estimated redshifts showing no or a slightly lower systematic offset increasing at the highest redshifts (e.g., Benoist et al. 2002; Olsen et al. 2005a; Olsen et al. 2005b). The scatter is found to be consistent with the spectroscopic results.

Lastly, we show the relative richness offsets ($[\Lambda_{\rm cl,out} - \Lambda_{\rm cl,in}]/\Lambda_{\rm cl,in}$) in the upper panel of Fig. 8. It can be seen that at low redshift there is an overestimate on average up to 100% and a slight underestimate at the highest redshifts, while at intermediate redshifts the average is in good agreement with the input richness. At all redshifts the scatter of the recovered richness is large. The richness estimate depends on the estimated redshift, therefore when the redshifts are overestimated we expect the same for the richness (an M^* galaxy at higher redshift has an apparent flux that is smaller than at lower redshift and therefore the equivalent number of M^* galaxies is larger). To investigate this effect, we corrected the measured richness to the value corresponding to the input redshift. This correction is made by multiplying the recovered richness by the flux ratio between an L^* galaxy at the recovered redshift to one at the input redshift. The result of this correction is shown in the lower panel of Fig. 8. It can be seen that most of the systematic offset is removed, thus we attribute the systematic offsets in the richness estimate to the offset in redshift.

Even though based on simple simulations, the present results will serve as a reference for future work investigating the effects of clusters that do not exactly resemble the model cluster. It is an important step for understanding the strengths and weaknesses of the detection under well-controlled conditions before adding the entire complexity of different cluster morphologies and superpositions through the use of N-body simulations.

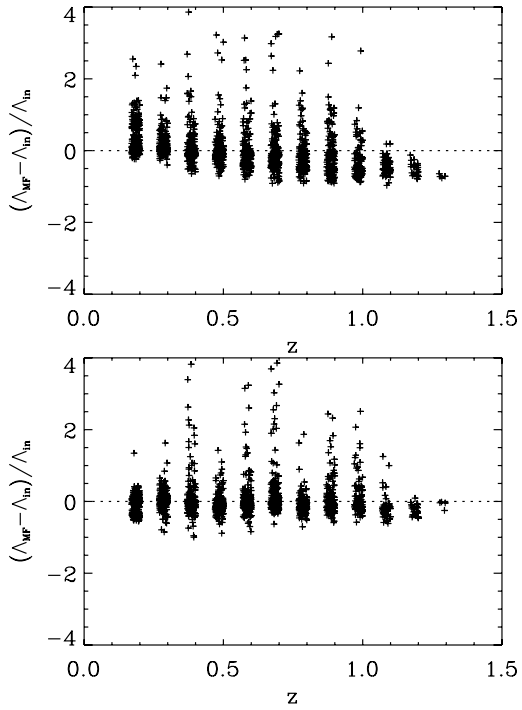

Fig. 8. The relative richness offsets as function of input redshift. The horizontal dashed line gives the zero offset line. The upper panel shows the measured relative offsets from the input values while the lower panels show the richness offsets after correcting for the redshift offsets as detailed in the text.

4. Application to the CFHTLS deep fields

The matched filter algorithm as described above was applied to the $i-$band catalogues of the four Deep CFHTLS fields. The resulting cluster candidate catalogue is presented in Table 3 giving the first five entries. The entire list is available at the CDS. The table lists in Col. 1 the cluster name, in Col. 2 and 3 the right ascension and declination in J2000, in Col. 4 the estimated redshift, in Col. 5 the $\Lambda_{\rm cl}$ richness, in Col. 6 the S/N of the peak value of the detection, in Col. 7 the number of redshift bins where the candidate was detected, in Col. 8 the fraction of lost area within a distance of $1h_{75}^{-1}$ Mpc from the cluster position and in Col. 9 the grade as defined below. The total number of detections is 162 corresponding to 52.1 per square degree for an effective area of ∼3.112 square degrees. From the density of detections in each field we compute the average density to be $\sim 52.1 \pm 7.8$ per square degree, where the error indicates the scatter between the four fields. From the simulated backgrounds we estimate to have $\sim 16.9 \pm 5.4$ false detections per square degree. This corresponds to a noise fraction of ∼32%. Below we compare the properties to results of other authors.

All the detected systems were visually inspected using the related *gri* and *grz* colour images. The candidates were split into four categories denoted by the following grades: grade A systems show a clear concentration of galaxies with similar colours; grade B systems are characterized by an overdensity of galaxies, less concentrated than grade A systems or without any obvious colour concentration; grade C systems do not reveal any clear galaxy overdensity; and finally grade D systems are systems that were detected because of lack of masking of the galaxy catalogue or because of an artefact due to the presence of an edge. The relative fractions of each grade are 38.3% for grade A, 37.0% for grade B, 22.8% for grade C and 1.9% for grade D. From these numbers we find that the density of grade A systems is ∼20 per square degree. It is worth noting that the fraction of grade C and D systems is slightly smaller than the estimated noise fraction possibly indicating that the correlated backgrounds indeed slightly overestimates the true noise frequency. However, some of the grade B systems may also be due to superposition effects and thus contribute to the noise of the catalogue.

In Figs. 9 and 10 we show the spatial distribution of cluster candidates for each field for redshifts $z_{\rm MF} \leq 0.6$ and $z_{\rm MF} \geq 0.7$, respectively. We show the masks (polygons) and the detected clusters (filled circles). The size of the circles reflects the estimated richness of the systems with larger circles indicating richer systems. It can be seen that the number of detections in each field varies in both redshift intervals.

In Fig. 11 we show the redshift and richness distributions and compare them to the estimated contribution from false-positives. For the redshift distribution the error bars indicate the field-to-field variation. To investigate the expected variance of the counts we used cluster samples extracted from *N*-body simulations (Evrard et al. 2002). From this paper we used the results of the ΛCDM simualtions and the deep wedge (DW) survey with a total (simulated) sky coverage of 10×10 square degrees and a maximum redshift of 4.4. The adopted mass limits are only rough estimates obtained from the conversion between $\Lambda_{\rm cl}$-richness and Abell richness class given in Table 2. To convert Abell richness classes to a mass limit we used the sample by Girardi et al. (1998). For each Abell richness class we computed the average mass and used this as our rough estimate. When extracting cluster samples from the *N*-body simulations we rescaled the mass threshold as a function of redshift to obtain samples with sizes similar to the density in the candidate catalogue. Extracting randomly from these simualtions sets of 4 realisations of 1 square degree yields a variance consistent with the field to field variation measured from the 4 Deep fields.

Finally, Fig. 12 shows the redshift and richness distributions indicating the contribution of grade A and B systems. It can be seen that the distributions are at any redshift and richness dominated by grade A and B systems which are both characterized by a clear overdensity of galaxies.

4.1. Statistical comparison to previous surveys

Even though the number of high-redshift cluster searches is still limited, a number of samples are available for comparison. First, we compare the present catalogue with that from the EIS project (Olsen et al. 1999a,b; Scodeggio et al. 1999) since the adopted method here is essentially the same but applied to another data set. Afterwards we compare with two other optical catalogues: the KPNO/Deeprange distant cluster survey using a different data set covering 16 square degrees also in the $I-$band and using a matched-filter algorithm (Postman et al. 2002) and the Red Sequence Cluster Survey (RCS; Gladders & Yee 2005) that used both a different data set and a different detection method, namely searching for simultaneous overdensities in colour and space.

In Fig. 13 we compare the distributions of the properties of cluster candidates in the CFHTLS catalogue presented here and those in the EIS cluster candidate catalogue. The difference between the surveys is both the passband (EIS used a wide $I-$band filter with a limiting magnitude of $I_{AB} \sim 23.4$, while in CFHTLS the more narrow Sloan $i-$band filter is used) and the depth of the data. Already this is expected to have some impact on the obtained cluster candidate samples, but in particular at low redshift, this is not expected to be a large effect. The two catalogues are built with essentially the same algorithm, however, it can be

Table 3. The first five entries of the cluster candidate catalogue. The entire table is available at CDS.

Name	α (J2000)	δ (J2000)	$z_{\rm MF}$	$\Lambda_{\rm cl}$	*S/N*	# Bins	Frac. of lost area	grade
CFHTLS-CL-J022410-041940	02:24:10.3	–04:19:40.7	0.9	79.5	4.32	3	0.10	A
CFHTLS-CL-J022411-042511	02:24:11.6	–04:25:11.1	1.1	123.0	4.10	2	0.08	C
CFHTLS-CL-J022413-040412	02:24:13.4	–04:04:12.7	1.1	120.1	4.01	2	0.01	B
CFHTLS-CL-J022423-044044	02:24:23.1	–04:40:44.3	0.4	27.2	4.27	3	0.03	B
CFHTLS-CL-J022423-044303	02:24:23.3	–04:43:03.6	0.5	29.1	3.90	4	0.02	A

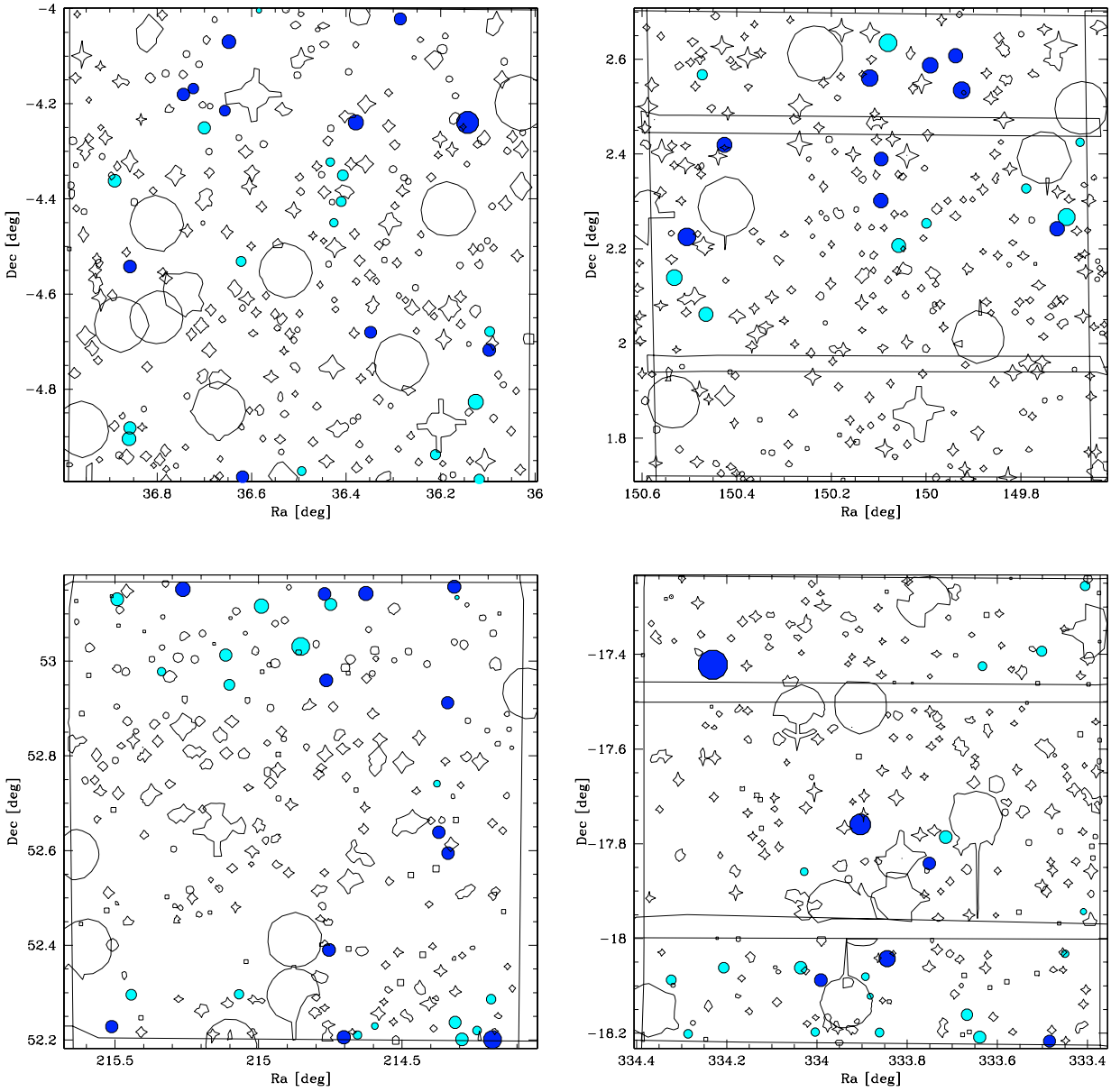

Fig. 9. The projected distribution of clusters with $z_{\rm MF} \leq 0.6$ (filled circles) detected in the four fields. The dark circles denote the grade A systems, while the grey ones indicate any other grade. The diameter of the circles increase with the richness of the cluster. The first row shows D1 (*left*) and D2 (*right*) and below are the fields D3 (*left*) and D4 (*right*). The additional polygons mark the position of masked regions.

seen that the CFHTLS includes more systems than the EIS sample at all redshift. The large difference is likely to result from the adopted detection thresholds, which is a major difference between the two detection procedures. In contrast to the present project, in EIS the detection thresholds were defined intrinsic to each field. For the richnesses (Fig. 14) we compare the detections in three different redshift bins, since the average richness increases with redshift (due to the selection function). Each line type corresponds to a different redshift range as indicated in the caption. In general the CFHTLS identifies a larger number of

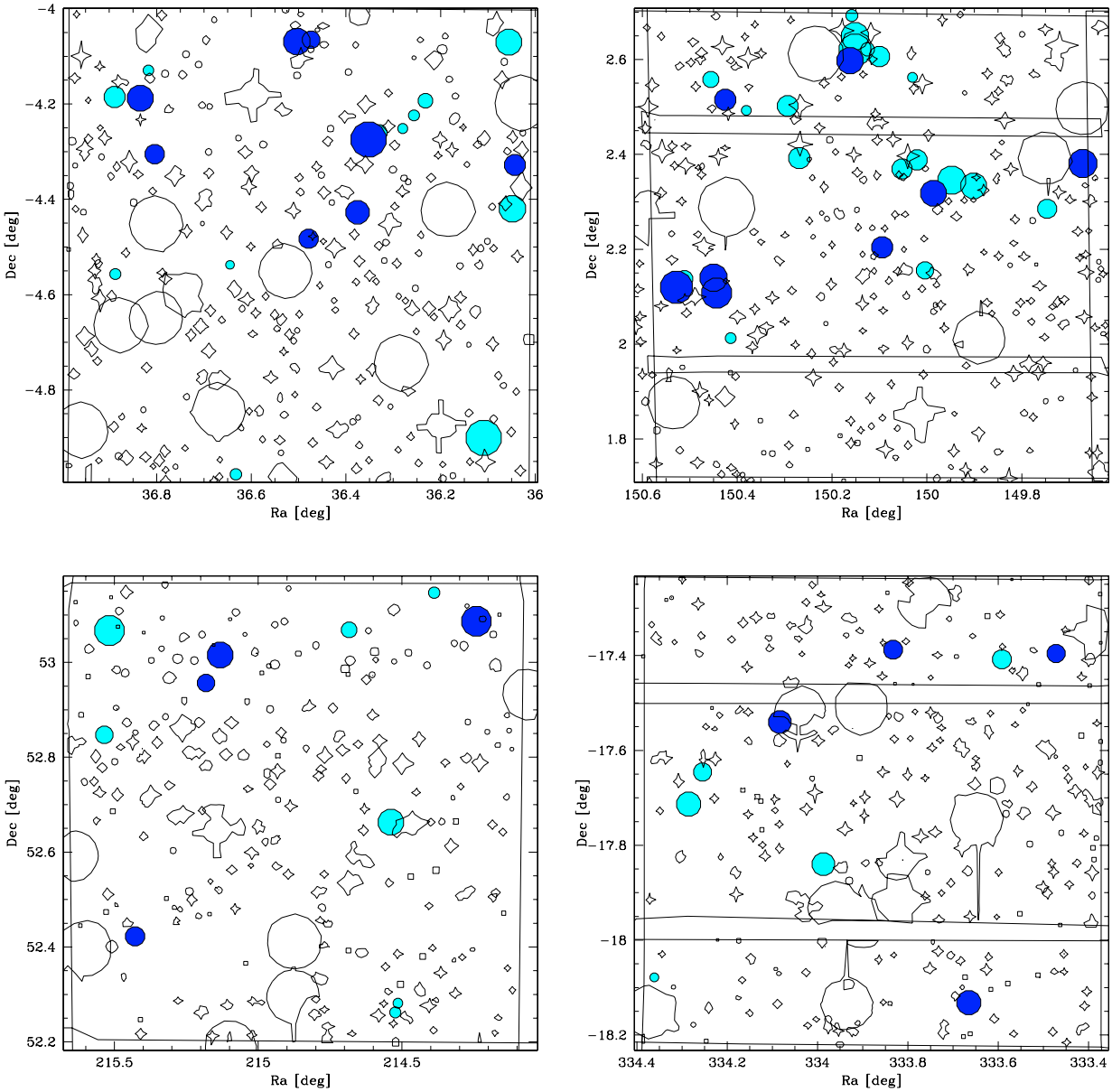

Fig. 10. Same as Fig. 9 but for clusters with $z_{\rm MF} \geq 0.7$.

poorer systems than was done in EIS which is probably a combination of the different detection thresholds and deeper data.

In Fig. 15 we compare the redshift distribution with that of the KPNO/Deeprange distant cluster survey (Postman et al. 2002) as well as that of the RCS (Gladders & Yee 2005). Both of these surveys are estimated to cover roughly the same redshift interval as in the present survey. We find that at most redshifts the CFHTLS distribution includes more systems than the KPNO/Deeprange catalogue, and is comparable to the distribution of the RCS. Since the RCS is using a different detection method also the definition of the richness of the detected systems differs and thus a direct comparison is not possible in this case.

For the three surveys where $\Lambda_{\rm cl}$-richnesses are available (CFHTLS, EIS and KPNO/Deeprange) we present the breakdown by richness in Table 4. The richness intervals are selected based on the values in Table 2 to correspond roughly to Abell richness classes $R \lesssim 0$, $R \sim 1$, $R \sim 2$ and $R \gtrsim 3$. From the table it can be seen that the additional detections in the CFHTLS catalogue is likely due to a larger number of relatively poor systems.

Table 4. For each of the three surveys the density of clusters (per square degree) in four different richness intervals. The richness intervals correspond roughly to Abell richness classes $R \lesssim 0$, $R \sim 1$, $R \sim 2$ and $R \gtrsim 3$.

Richness	CFHTLS	EIS	Deeprange
$\Lambda_{\rm cl} < 35$ ($R \lesssim 0$)	22.5	3.6	4.2
$35 \leq \Lambda_{\rm cl} < 75$ ($R \sim 1$)	18.3	10.5	15.9
$75 \leq \Lambda_{\rm cl} < 125$ ($R \sim 2$)	9.3	2.6	7.0
$125 \leq \Lambda_{\rm cl}$ ($R \gtrsim 3$)	1.9	4.3	0.6

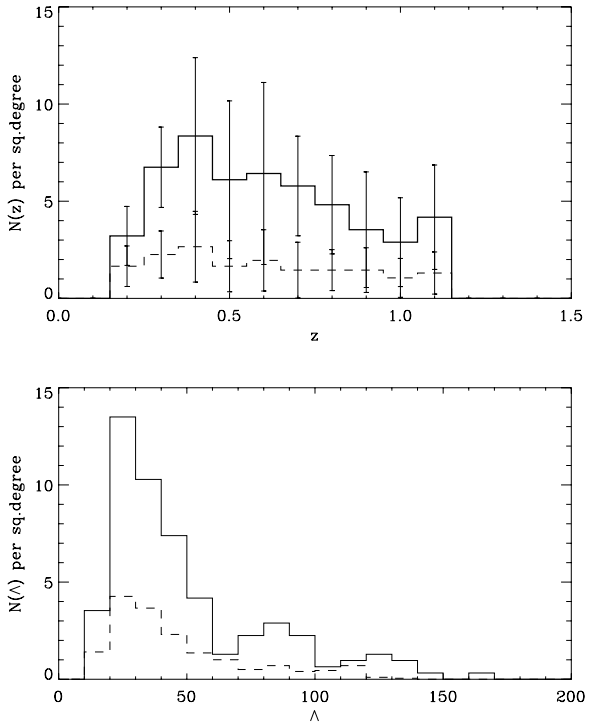

Fig. 11. Redshift (*top*) and richness (*lower*) distributions (solid lines) for all the candidate clusters. The distributions of false detections (dashed lines) are estimated using the correlated backgrounds. For the redshift distribution the error bars denote the scatter between the fields.

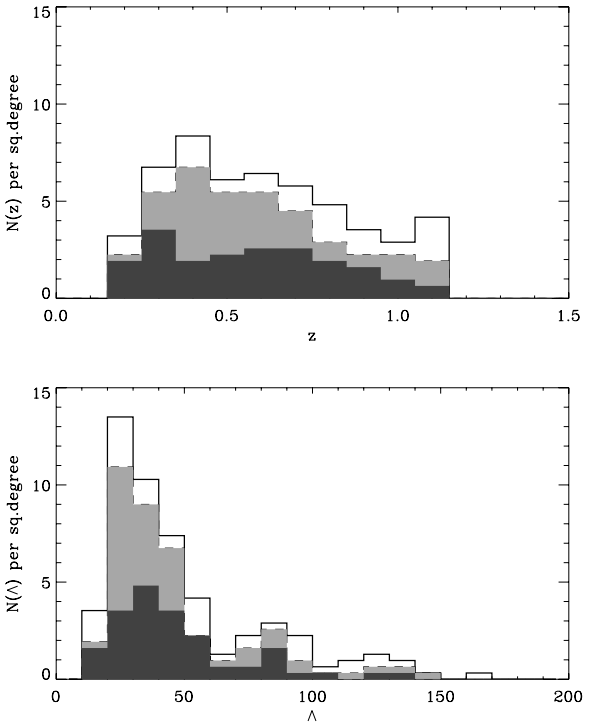

Fig. 12. Redshift (*top*) and richness (*lower*) distributions for all the candidate clusters (solid lines) and marking the grade A (dark grey) and B (light grey) systems.

4.2. Direct comparison to other samples

A number of clusters are already known in the investigated areas. In order to estimate the accuracy of the estimated redshifts as well as compare the properties of clusters identified by different methods, we use NASA/IPAC Extragalactic Database (NED) to find clusters with known spectrocsopic redshifts. All of these are found to be X-ray identified systems. The main source of externally detected clusters is the XMM-LSS (Valtchanov et al. 2004; Andreon et al. 2005; Willis et al. 2005; Pierre et al. 2006) covering the Deep-1 field. In addition one detection from the ROSAT Bright Source Catalog Sample (Bauer et al. 2000) is located in the Deep-4 field.

In Table 5 we list the previously spectroscopically confirmed clusters found in the areas searched in the present work. The table lists in Col. 1 a cluster id, in Cols. 2 and 3 the position in J2000, in Col. 4 the external spectroscopic redshift, in Col. 5 the matched filter redshift when there is a match, in Col. 6 a flag whether the cluster position falls within a mask and in Col. 7 the reference(s) of the external position of the cluster.

In the XMM-LSS catalogues of the D1 field (Andreon et al. 2005; Willis et al. 2005; Pierre et al. 2006) we find a total of 17 detections. When comparing to our catalogue, we find all but 5 of these detections. Of those 5 two are masked and the remaining three systems are optically poor.

For the 12 XMM-LSS systems where we find a counterpart and the ROSAT cluster we compute the average redshift offsets. We find a mean offset of $z - z_{\rm MF} = -0.05$ with a scatter of 0.14. Among the 13 systems one shows an offset of $\Delta z = -0.32$. For this system the colour image shows the presence of two galaxy concentrations. The XMM-LSS position is located between the two concentrations, while that of the present survey corresponds to the one most distant from the XMM-LSS detection. Thus the matching of this case is ambiguous. Discarding this case leads to an average redshift offset of $\Delta z = -0.02$ with a scatter of 0.12. This is consistent with the offsets estimated from the simulations in Sect. 3.3.

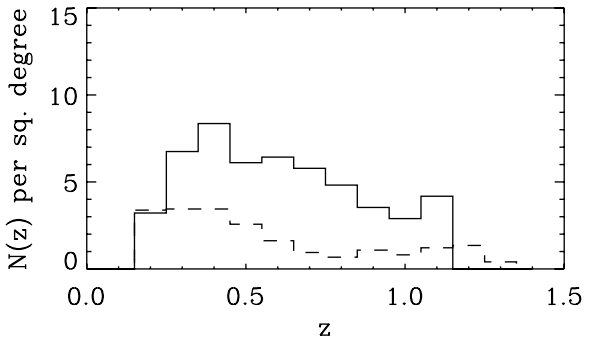

Fig. 13. Comparison of redshift distributions for the CFHTLS (solid line) and EIS (dashed line) cluster catalogues (Olsen et al. 1999a,b; Scodeggio et al. 1999).

All of the matched XMM-LSS systems are graded A in our catalogue. However, the geometry of the XMM-LSS survey does not allow a complete coverage of the D1 field. Therefore, we investigate the position of our 9 remaining grade A systems with respect to the XMM-LSS pointings (Pierre et al. 2006). Of these nine systems 3 are not covered by any XMM-LSS pointing and 4 are found at the edge of a pointing. The last 2 systems are located in XMM-LSS pointings G01 and G02, where the G02 pointing is significantly shallower than the other pointings. The candidate detected by our search in G01 is at $z_{\rm MF} = 0.4$ and $\Lambda_{\rm cl} = 29$, thus not a very rich system. Also the visual inspection of this candidate shows that the system is poor, even though a nice concentration in colour and space is seen. Altogether, considering only our grade A systems and the overlap with the XMM-LSS

Table 5. Spectroscopically confirmed X-ray clusters in the four surveyed fields.

Id	RA	Dec	z_{spec}	z_{MF}	Masked	Ref.
XLSSC029	36.0172	–4.2247	1.05	–	Y	1, 3
XLSSC044	36.1410	–4.2376	0.26	0.3	N	1
XLSSJ022522.7-042648	36.3454	–4.4468	0.46	–	N	1
XLSSC025	36.3526	–4.6791	0.26	0.3	N	1
XLSSJ022529.6-042547	36.3733	–4.4297	0.92	0.8	N	1
XLSSC041	36.3777	–4.2388	0.14	0.3	N	1
XLSSC011	36.5403	–4.9684	0.05	0.2	Y	1
XLSSJ022609.9-043120	36.5421	–4.5226	0.82	–	N	1
XLSSC017	36.6174	–4.9967	0.382	0.5	Y	4
XLSSC014	36.6411	–4.0633	0.344	0.4	N	4
XLSSJ022651.8-040956	36.7164	–4.1661	0.34	0.3	N	1
XLSSC005	36.7877	–4.3002	1.05	0.9	N	1, 2, 3
XLSSC038	36.8536	–4.1920	0.58	0.9	N	1
XLSSC013	36.8588	–4.5380	0.31	0.3	N	1, 4
XLSSC022	36.9178	–4.8586	0.29	–	Y	1
XLSSJ022534.2-042535	36.3925	–4.42639	0.92	0.8	N	3
XLSSC005b	36.800	–4.23056	1.0	–	N	3
RBS1842	334.23917	–17.42444	0.136	0.2	N	6

1. Pierre et al. (2006), 2. Valtchanov et al. (2004), 3. Andreon et al. (2005), 4. Willis et al. (2005), 5. Bauer et al. (2000).

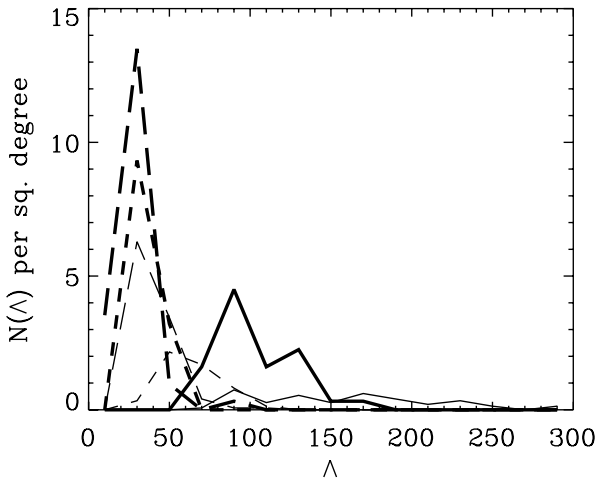

Fig. 14. Comparison of richness distributions for the CFHTLS (thick lines) and EIS (thin lines) cluster catalogues (Olsen et al. 1999a,b; Scodeggio et al. 1999). Each line correspond to a redshift interval as follows: long-dashed line $0.2 \leq z \leq 0.4$, short-dashed line $0.5 \leq z \leq 0.7$ and solid $0.8 \leq z \leq 1.1$.

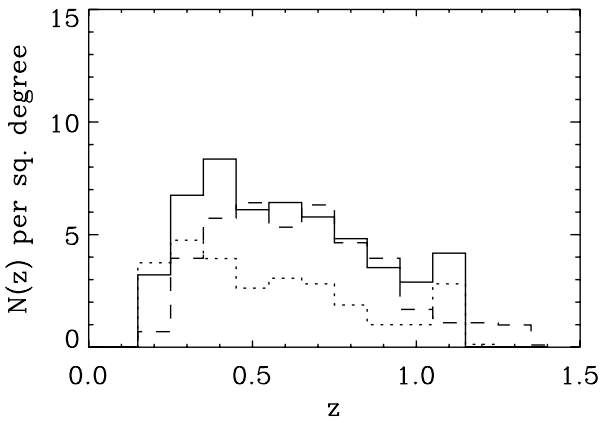

Fig. 15. Comparison of redshift distributions for the CFHTLS (solid line), KPNO/Deeprange (dotted line, Postman et al. 2002) and RCS (dashed line, Gladders & Yee 2005) cluster catalogues.

survey, the two catalogues are in good agreement. In addition, the present sample contains a number of systems in the same area graded B or C for which there is no known X-ray counterparts. However, from the visual inspection of the images we expect that more detailed invesigations will show that a number of them corresponds to physical systems.

5. Summary

In this paper we present the first catalogue of optical cluster candidates extracted from the CFHTLS Deep data. Using an improved implementation of the matched-filter procedure of the EIS project (Olsen et al. 1999a) we construct cluster catalogues in the $i-$band for the Deep fields of the present survey. Through simple simulations we assess the rate of false detections as well as the recovery rate. The main properties of the catalogue are the following:

- The catalogue contains 162 clusters covering the redshift range from $z = 0.2$ to 1.1 with a median of $z_{med} = 0.6$. The density of candidates is 52.1 ± 7.8 per square degree; among them, ∼20 per square degree show a concentration of similarly coloured galaxies.
- The estimated rate of false detections is ∼16.9 ± 5.4 per square degree. This density is consistent with the fraction of systems not showing any obvious concentration in the visual inspection.
- From simulations we find that the catalogue is complete for systems of richness class ≥ 1 up to $z = 0.7$; beyond that the recovery rate decreases to close to zero at $z \sim 1.2$.
- We find that the estimated redshifts are in general overestimated by $\Delta z \sim 0.1$ with a scatter of $\sigma_{\Delta z} \sim 0.1$. Correcting for this redshift offset, the recovered richnesses are in good agreement with the input.

– The present catalogue extracted from the CFHTLS Deep fields appears to trace poorer systems at higher redshifts than previous matched-filter cluster catalogues.

We have compared our catalogue with that of the XMM-LSS survey (Pierre et al. 2006). From this comparison we found that our grade A systems in the region of overlap between the two surveys were detected by XMM-LSS. The remaining X-ray detections that were not included in our catalogue were either in masked regions or appeared optically poor. The grade B and C systems were not included in the known (X-ray) cluster samples.

We conclude that, the CFHTLS imaging survey provides a good basis for constructing large samples of galaxy clusters to study the evolution of cluster properties as well as for other cosmological applications. Furthermore, the ability to trace the poor cluster population may allow for studying the processes of cluster growth and their impact on the galaxy populations and evolution in more detail than with previous samples. In order to gain a better understanding of the detected systems we will use photometric redshifts to investigate their properties. However, to fully describe their nature we have to carry out a thorough spectroscopic follow-up.

Acknowledgements. We thank the referee, Peter Schuecker, for useful comments, which helped improving the manuscript. During the work we have benefitted from useful discussions with S. Arnouts, R. Gavazzi and G. Soucail. This work is based on observations obtained with MegaPrime/MegaCam, a joint project of CFHT and CEA/DAPNIA, at the Canada-France-Hawaii Telescope (CFHT) which is operated by the National Research Council (NRC) of Canada, the Institut National des Science de l'Univers of the Centre National de la Recherche Scientifique (CNRS) of France, and the University of Hawaii. This work is based in part on data products produced at TERAPIX and the Canadian Astronomy Data Centre as part of the Canada-France-Hawaii Telescope Legacy Survey, a collaborative project of NRC and CNRS. This research has made use of the NASA/IPAC Extragalactic Database (NED) which is operated by the Jet Propulsion Laboratory, California Institute of Technology, under contract with the National Aeronautics and Space Administration. We thank the French Programme National de Cosmologie for its support to the CFHTLS galaxy cluster program. LFO acknowledges financial support from the Danish Natural Sciences Research Council and the Poincaré fellowship program at Observatoire de la Côte d'Azur. The Dark Cosmology Centre is funded by the Danish National Research Foundation. CB thanks the Dark Cosmology Centre for hospitality during the final stages of this work. AC acknowledges visitor support from the CNRS through a *poste rouge* and the Observatoire de la Côte d'Azur for its hospitality.

References

Andreon, S., Valtchanov, I., Jones, L. R., et al. 2005, MNRAS, 359, 1250
Bahcall, N. 1988, ARA&A, 26, 631
Bahcall, N., Fan, X., & Cen, R. 1997, ApJ, 485, L53
Bahcall, N., McKay, T., Annis, J., et al. 2003, ApJS, 148, 243
Bauer, F. E., Condon, J. J., Thuan, T. X., & Broderick, J. J. 2000, ApJS, 129, 547
Benoist, C., da Costa, L., Jørgensen, H., et al. 2002, A&A, 394, 1
Bertin, E., & Arnouts, S. 1996, A&AS, 117, 393
Böhringer, H., Voges, W., Huchra, J. P., et al. 2000, ApJS, 129, 435
Böhringer, H., Schuecker, P., Guzzo, L., et al. 2004, A&A, 425, 367
Carlstrom, J. E., Holder, G. P., & Reese, E. D. 2002, ARAA, 40, 643
Coleman, G., Wu, C.-C., & Weedman, D. 1980, ApJS, 43, 393
Collins, C., Guzzo, L., Böhringer, H., et al. 2000, MNRAS, 319, 939
De Propris, R., Couch, W. J., Colless, M., et al. 2002, MNRAS, 329, 87
Evrard, A. E., MacFarland, T. J., Couchman, H. M. P., et al. 2002, ApJ, 573, 7
Gal, R. R., de Carvalho, R. R., Lopes, P. A. A., et al. 2003, AJ, 125, 2064
Gavazzi, R., & Soucail, G. 2006, A&A, submitted [arXviv:astro-ph/0605591]
Girardi, M., Giuricin, G., Mardirossian, F., Mezzetti, M., & Boschin, W. 1998, ApJ, 505, 74
Gladders, M., & Yee, H. 2001, in The New Era of Wide Field Astronomy (Astronomical Society of the Pacific), ASP Conf. Ser., 232, 126
Gladders, M., & Yee, H. 2005, ApJS, 157, 1
Goto, T., Sekiguchi, M., Nichol, R., et al. 2002, AJ, 123, 1807
Holder, G., Haiman, Z., & Mohr, J. 2001, ApJ, 560, L111
Huchra, J., Geller, M., Patrick, H., & Postman, M. 1990, ApJ, 365, 66
Kepner, J., Fan, X., Bahcall, N., Gunn, J., & Lupton, R. 1999, ApJ, 517, 78
Kim, R., Kepner, J., Postman, M., et al. 2002, AJ, 123, 20
Lidman, C., Rosati, P., Demarco, R., et al. 2004, A&A, 416, 829
Lobo, C., Iovino, A., Lazzati, D., & Chincarini, G. 2000, A&A, 360, 896
Miller, C. J., Nichol, R. C., Reichart, D., et al. 2005, AJ, 130, 968
Olsen, L. F., Scodeggio, M., da Costa, L., et al. 1999a, A&A, 345, 681
Olsen, L. F., Scodeggio, M., da Costa, L., et al. 1999b, A&A, 345, 363
Olsen, L. F., Benoist, C., da Costa, L., Hansen, L., & Jørgensen, H. 2005a, A&A, 435, 781
Olsen, L. F., Zucca, E., Bardelli, S., et al. 2005b, A&A, 442, 841
Oukbir, J., & Blanchard, A. 1997, A&A, 317, 1
Pierre, M., Pacaud, F., Duc, P.-A., et al. 2006, MNRAS, accepted [arXiv:astro-ph/0607170]
Popesso, P., Böhringer, H., Romaniello, M., & Voges, W. 2005, A&A, 433, 415
Postman, M., Lubin, L., Gunn, J., et al. 1996, AJ, 111, 615
Postman, M., Lauer, T., Oegerle, W., & Donahue, M. 2002, ApJ, 579, 93
Schechter, P. 1976, ApJ, 203, 297
Schlegel, D., Finkbeiner, D., & Davis, M. 1998, ApJ, 500, 525
Schuecker, P., & Böhringer, H. 1998, A&A, 339, 315
Schuecker, P., Böhringer, H., Collins, C., & Guzzo, L. 2003, A&A, 398, 867
Scodeggio, M., Olsen, L. F., da Costa, L., et al. 1999, A&AS, 137, 83
Soneira, R. M., & Peebles, P. J. E. 1978, AJ, 83, 845
Stanford, S., Elston, R., Eisenhardt, P., et al. 1997, AJ, 114, 2232
Stanford, S., Eisenhardt, P., & Dickinson, M. 1998, ApJ, 492, 461
Szalay, A., Connolly, A., & Szokoly, G. 1999, AJ, 117, 68
Tago, E., Einasto, J., Saar, E., et al. 2006, Astron. Nachr., 327, 365
Valtchanov, I., Pierre, M., Willis, J., et al. 2004, A&A, 423, 75
van Dokkum, P., & Franx, M. 2001, ApJ, 553, 90
van Dokkum, P., Franx, M., Fabricant, D., Illingworth, G., & Kelson, D. 2000, ApJ, 541, 95
Willis, J. P., Pacaud, F., Valtchanov, I., et al. 2005, MNRAS, 363, 675